Identification of Novel ROS Inducers: Quinone Derivatives Tethered to Long Hydrocarbon Chains

Yeonsun Hong,[†,§] Sandip Sengupta,[‡,§] Wooyoung Hur,*[‡] and Taebo Sim*[†,‡]

[†]KU-KIST Graduate School of Converging Science and Technology, 145 Anam-ro, Seongbuk-gu, Seoul, 136-713, Republic of Korea

[‡]Chemical Kinomics Research Center, Korea Institute of Science and Technology (KIST), 5 Hwarangro 14-gil, Seongbuk-gu, Seoul, 136-791, Republic of Korea

S *Supporting Information*

Irisferin A
proposed structure

Strong ROS inducer
Potent anti-cancer agent

ROS
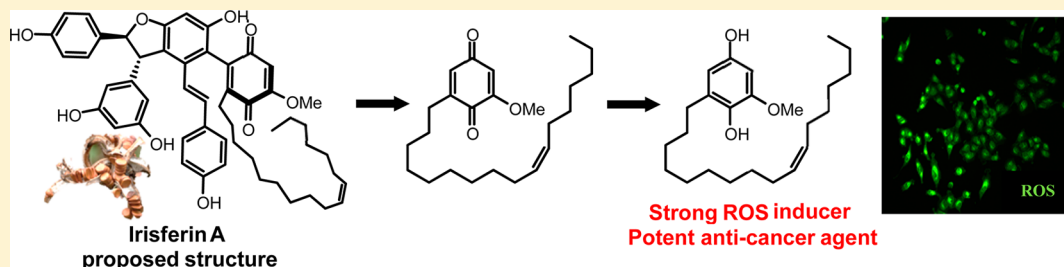
ABSTRACT: We performed the first synthesis of the 17-carbon chain-tethered quinone moiety **22** (SAN5201) of irisferin A, a natural product exhibiting anticancer activity, and its derivatives. We found that **22** is a potent ROS inducer and cytotoxic agent. Compound **25** (SAN7401), the hydroquinone form of **22**, induced a significant release of intracellular ROS and apoptosis (EC_{50} = 1.3−2.6 μM) in cancer cell lines, including A549 and HCT-116. Compared with the activity of a well-known ROS inducer, piperlongumine, **22** and **25** showed stronger cytotoxicity and higher selectivity over noncancerous cells. Another hydroquinone tethering 12-carbon chain, **26** (SAN4601), generated reduced levels of ROS but showed more potent cytotoxicity (EC_{50} = 0.8−1.6 μM) in cancer cells, although it lacked selectivity over noncancerous cells, implying that the naturally occurring 17-carbon chain is also crucial for ROS production and a selective anticancer effect. Both **25** and **26** displayed strong, equipotent activities against vemurafenib-resistant SK-Mel2 melanoma cells and p53-deficient H1299 lung cancer cells as well, demonstrating their broad therapeutic potential as anticancer agents.

INTRODUCTION

Natural products have been a rich source of anticancer drugs and inspired the development of a number of drugs having novel scaffolds. Natural product-based chemical entities account for almost 60% of anticancer drugs and show their efficacy mainly through modulating cancer-related signaling pathways, such as the p53 and MAPK pathways.[1,2]

Irisferin A is a resveratrol derivative isolated from the seed extract of *Iris pseudacorus* (Iridaceae) that is utilized as a traditional herbal medicine in Korea. A group in Korea proposed the structure of irisferin A (Figure 1) and reported that irisferin A is capable of suppressing proliferation of human cancer cell lines, including SK-Mel2 (EC_{50} = 1.38 μM) and A549 (EC_{50} = 4.65 μM).[3] The antiproliferative activity against SK-Mel2 melanoma cells is noteworthy because SK-Mel2 cells are resistant to FDA-approved B-Raf[V600E] inhibitor vemurafenib.[4] Thus, it has become a crucial issue in targeted melanoma therapy to identify novel small molecules that override vemurafenib resistance.[5,6]

Cancer cells are exposed to a relatively high level of reactive oxygen species (ROS) compared to that for normal cells, primarily due to their active metabolism driven by oncogenic signals.[7] In fact, cancer cells take advantage of this moderate oxidative stress for several important processes such as proliferation, angiogenesis, and metastasis.[8] However, excessive ROS levels irreversibly damage DNA and lipids and ultimately cause apoptosis of cancer cells.[9] Recently, pharmacological elevation of intracellular ROS emerged as an effective strategy for selectively targeting cancer cells. An exogenous ROS insult that is within a tolerable level to normal cells could exceed the threshold that cancer cells can endure, leading to selective eradication of cancer cells.[7,10,11] Moreover, the efficacy of this redox-modulating method has been demonstrated in models of drug-resistant cancers as well.[12]

A number of small molecule ROS inducers have been discovered with diverse functional groups, including Michael acceptors, disulfides, isothiocyanates, and phenolic antioxidants.[9,12] They enhance ROS levels in cells mainly through their intrinsic redox chemistry, inhibition of intracellular antioxidant proteins, or perturbation of mitochondrial redox proteins. Recently, several ROS inducers, including piperlongumine and lanpersone, have been demonstrated that kill cancer cells with good selectivity over noncancerous cells.[13−15] Herein,
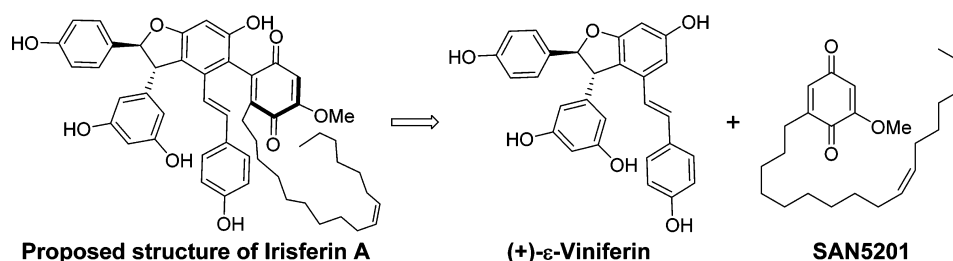
Figure 1. Proposed structure of irisferin A.

we report the quinone moiety of a natural product, irisferin A, and its derivatives as novel ROS inducers and introduce the analogues that possess potent anticancer activity with decent selectivity over noncancerous cells.

RESULTS AND DISCUSSION

Chemistry. Irisferin A consists of (+)-ε-viniferin and the hydrocarbon-tethered quinone moiety **22** (SAN5201), and the two moieties are linked through a C−C bond (Figure 1). We hypothesized that there might be a local pharmacophore within irisferin A responsible for its antiproliferative activity. In order to find the structural element critical for this activity, we assessed the two moieties separately.

The quinone moiety, **22**, and its derivatives were synthesized as shown in Scheme 1. Our synthesis began with commercially available 3,5-dimethoxybenzyl bromide **8**, which was transformed to the corresponding phosphonium salt (**9**) at 95% yield. We also prepared the benzyloxy aldehydes bearing two different carbon chain lengths. Two diols (**1** and **2**) were monoprotected with a benzyl group in moderate yields, and the remaining free hydroxyl group was oxidized by PCC to afford the desired aldehydes (**3** and **4**).

Wittig reaction between the phosphonium salt **9** and the benzyloxy aldehydes (**3** and **4**) using n-BuLi at 0 °C furnished mixtures of the corresponding cis/trans olefins (**10** and **11**) in 75 and 72% yields, respectively. Double bond reduction and benzyl group deprotection on the olefins were simultaneously carried out by Pd/C-catalyzed hydrogenation to yield the corresponding primary alcohols (**12** and **13**) in 91 and 94% yields. Swern oxidation followed by Wittig reaction with phosphonium salt **6** using t-BuOK resulted in the desired cis olefins (**16** and **17**) as sole products in 65−68% yields for two steps, whereas Swern oxidation followed by modified Julia olefination with sulfone **7** using KHMDS as a base resulted in the trans olefin (**18**) as the sole product in 68% yield over 2 steps.

Crucial methoxyphenol intermediates (**19**, **20**, and **21**) were successfully obtained through selective monodemethylation using NaH/C₂H₅SH in DMF in 92−95% yields. Oxidation reaction using catalytic salcomine and oxygen bubbling for 24 h afforded the desired quinone compounds (**22**, **23**, and **24**) in 41 to 42% yields. The quinones were reduced to the corresponding hydroquinones (**25**, **26**, and **27**) using stoichiometric sodium hydrosulfite in THF/MeOH/H₂O (2:2:1) in 61 to 62% yields. Hydroquinone **25** (SAN7401) was methylated using MeI/K₂CO₃ to afford **28** in 82% yield. Hydroquinone **26** (SAN4601) was hydrogenated using Pd/C catalyst to furnish **29** in 98% yield.

In order to synthesize dimethoxy (hydro)quinone derivatives, methoxyphenol intermediate **19** was brominated regioselectively using NBS in carbon tetrachloride at room temperature to afford **30** in 85% yield. The oxidation process using catalytic salcomine and oxygen bubbling was then employed to obtain bromo-quinone **31** in 38% yield. The bromo functionality was then converted to the methoxy group using Pd(PPh₃)₄ and Na₂CO₃ to yield **32** in 65% yield. Quinone **32** was reduced to hydroquinone **33** using stoichiometric sodium hydrosulfite in THF/MeOH/H₂O (2:2:1) in 51% yield. Also, quinone **32** was demethylated regioselectively using perchloric acid (60%) in CH₂Cl₂ to obtain hydroxyl quinone **34** in 83% yield.

Biological Evaluations. We measured the antiproliferative activities of these compounds using an MTT assay against four cancer cell lines: SK-Mel2 (B-Raf^WT melanoma), A375 (B-Raf^V600E melanoma), A549 (non-small cell lung cancer), and HCT-116 (colon cancer) cells. HFF-1 fibroblast cells, HaCaT keratinocytes, and MCF10A breast epithelial cells were also employed as noncancerous cells. We found that (±)-ε-viniferin possessed no antiproliferative activity against all four cancer cell lines, whereas **22** showed potent activities (EC₅₀ = 3.3−5.5 μM). Therefore, we envisioned that the anticancer activity of irisferin A might be attributed to **22**. Although we cannot completely rule out the active function of (+)-ε-viniferin for irisferin A, we focused on structure−activity relationship (SAR) analysis of **22**, as we observed antiproliferative activity solely from **22**.

The SAR with respect to cytotoxicity was similar for the four cancer cell lines. (Hydro)quinones bearing the 17-carbon chain showed a higher level of potency against cancer cells than against three noncancerous cell lines (Table 1). We also found that, compared with **22**, its hydroquinone form **25** showed slightly better cellular activities (EC₅₀ = 1.3−2.6 μM). Phenolic analogue **19** had significantly lower activity and dimethoxybenzene analogue **33** showed even lower cytotoxicity than that of **25**. Installation of an extra hydroxy (**34**) or methoxy group (**32**, **33**) to the (hydro)quinone ring significantly reduced the activity. Despite the decreased activity, however, **32**, **33**, and **34** maintained fairly good cytotoxicity (EC₅₀ = 5.1−7.8 μM), particularly against SK-Mel2 melanoma cells, and showed about 12−15-fold selectivity over HFF-1 noncancerous fibroblasts. In addition, 2-methoxyhydroquinone itself showed no cellular activity, suggesting that the 17-carbon chain is critical for cellular activity. This implies that the anticancer activity of the compounds might be mediated in part through direct interaction with certain intracellular targets.

We also found that when we replaced the 17-carbon chain of **22** and **25** with a 12-carbon chain, the resulting compounds (**23**, **26**) showed slightly better antiproliferative activity against the cancer cell lines but with little selectivity over noncancerous cells. This indicates that the 17-carbon chain of irisferin A might be crucial for mediating the selective anticancer effect. In addition, there was little change in cytotoxicity when the cis-internal olefin of **26** was changed to the trans form (**27**) or
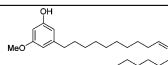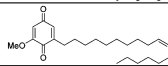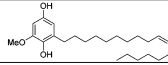
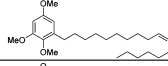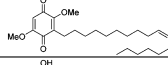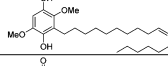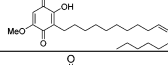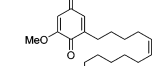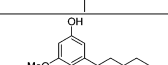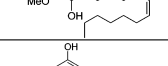**Scheme 1. Synthesis of the Quinone Moiety of Irisferin A and Its Derivatives**
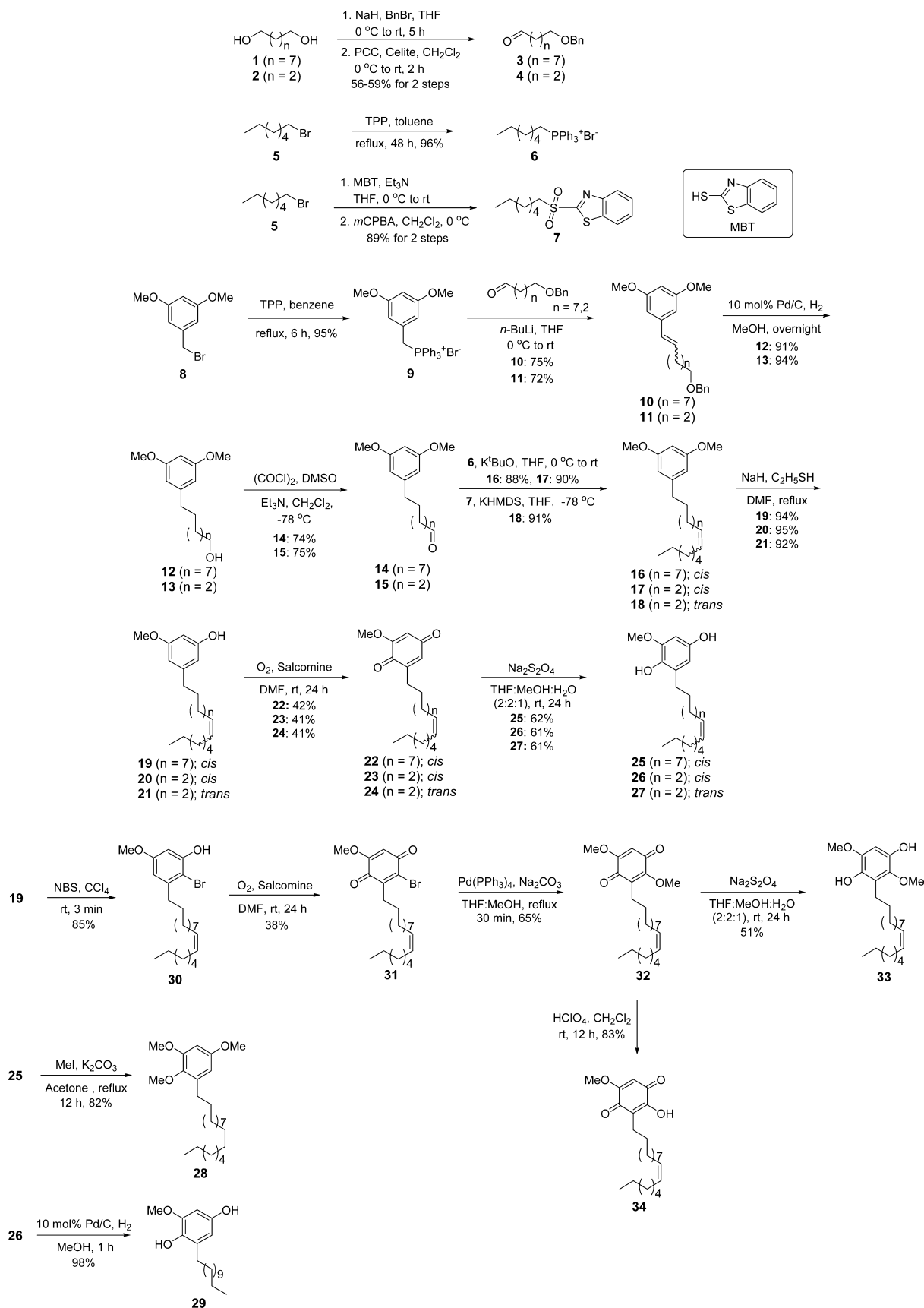
saturated (**29**), indicating that the geometry of the 12-carbon chain does not affect the cellular activity.

The two hydroquinones, **25** and **26**, turned out to be the most potent analogues against the cancer cells among all

Table 1. Antiproliferative Activity (EC$_{50}$'s, μM) of 22 and Its Derivatives against Four Cancer Cell Lines and Three Noncancerous Cell Lines^a

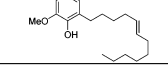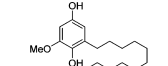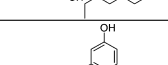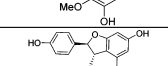| Compound	Structure	Cancer cells				Non-cancerous cells		
		A375	A549	HCT-116	SK-Mel2	HFF-1	HaCaT	MCF10A
19		19.2±0.2	22.7±3.9	16.3±1.3	17.9±4.07	19.2±1.1	17.2±0.4	15.6±1.3
22		5.52±2.54	3.25±0.78	4.19±1.34	4.40±1.20	14.8±2.7	11.4±1.3	26.4±3.0
25		2.60±0.72	1.29±0.66	1.47±0.66	2.35±0.81	7.72±1.28	3.95±0.93	10.8±1.6
28		42.6±2.7	43.0±1.6	45.3±16.2	36.9±13.4	>100	48.5±11.2	>100
32		16.1±4.8	13.0±3.0	15.2±3.2	7.79±2.78	95.5±11.3	48.8±4.5	34.7±7.2
33		12.2±3.2	10.7±1.8	8.07±2.34	5.08±1.71	82.7±9.9	40.6±5.3	23.1±2.7
34		23.7±7.0	16.8±3.8	17.5±5.9	6.24±1.29	>100	36.6±5.8	32.7±3.8
23		1.00±0.16	2.20±0.21	1.22±0.14	1.64±0.31	1.87±0.13	1.13±0.19	2.39±0.22
26		0.76±0.13	1.00±0.28	1.08±0.34	1.57±0.39	3.74±1.98	1.13±0.17	1.56±0.13
27		1.29±0.64	1.79±0.24	1.61±0.14	1.67±0.44	1.14±0.27	0.97±0.06	2.24±0.75
29		1.36±0.96	1.74±0.25	1.87±0.18	1.43±0.25	1.46±0.55	1.58±0.39	1.71±0.38
2-methoxyhydroquinone		>100	>100	>100	>100	>100	n.d.	>100
(±)-ε-viniferin		>100	>100	>100	>100	n.d.	n.d.	n.d.
piperlongumine		6.17±0.58	12.2±1.2	11.5±1.7	4.39±1.59	13.1±2.4	4.46±0.37	18.1±0.7

^{a}Data is presented as the mean and standard deviation obtained from three independent experiments. n.d., not determined.

derivatives having the 17-carbon chain and the 12-carbon chain, respectively. It is noteworthy that compound **25** showed stronger anticancer activities (EC$_{50}$ = 1.3−2.6 μM) and higher selectivity over noncancerous cells compared with that of a well-known ROS inducer, piperlongumine. Compound **26** exhibited stronger antiproliferative activities than **25** against the cancer cell lines (EC$_{50}$ = 0.8−1.6 μM). Because **25** and **26** were most potent against A549 and HCT116 cells, we used these two cancer cell lines for detailed analysis.

Several studies have demonstrated that resveratrol derivatives and fatty acids are able to generate ROS in cells.[16,17] Since the proposed structure of irisferin A contains both a resveratrol derivative and a lipophilic long hydrocarbon chain, we first investigated whether our synthetic analogues are able to generate ROS in A549 cells. We monitored intracellular ROS level using a ROS-sensitive fluorogenic dye (dichlorodihydro-fluorescein diacetate, DCF-DA) after treating the cells with compounds (2 and 10 μM) for 3 h. Imaging analysis revealed that **22** strongly generated ROS in A549 cells, and its hydroquinone form **25** induced ROS more profoundly. We

observed moderate ROS generation from **26**, **27**, and **29**, and almost no ROS induction from the remaining compounds (Figure 2A).

We observed that hydroquinone analogues generated higher ROS than their corresponding quinones. This is consistent with the well-known concept that quinones are bioreduced and the resulting hydroquinones act as the active species for intracellular ROS generation. When we installed an extra electron-donating group (hydroxyl or methoxy group) on the (hydro)quinone ring, ROS generation and antiproliferative activity were greatly decreased. The electron-donating substituents on hydroquinone might prohibit the tendency to transfer a single electron to molecular oxygen or might render the enol form (hydroquinone) disfavored between keto−enol equilibrium, resulting in reduced ROS generation.[18] Moreover, **25** and **26** generated a more intense ROS signal in A549 lung cancer cells than in noncancerous HFF-1 cells (Figure 2B). Particularly, **25** showed ROS generation in A549 cells but barely promoted the release of ROS in HFF-1 cells. This suggests that selective cytotoxicity of **25** against A549 cells over
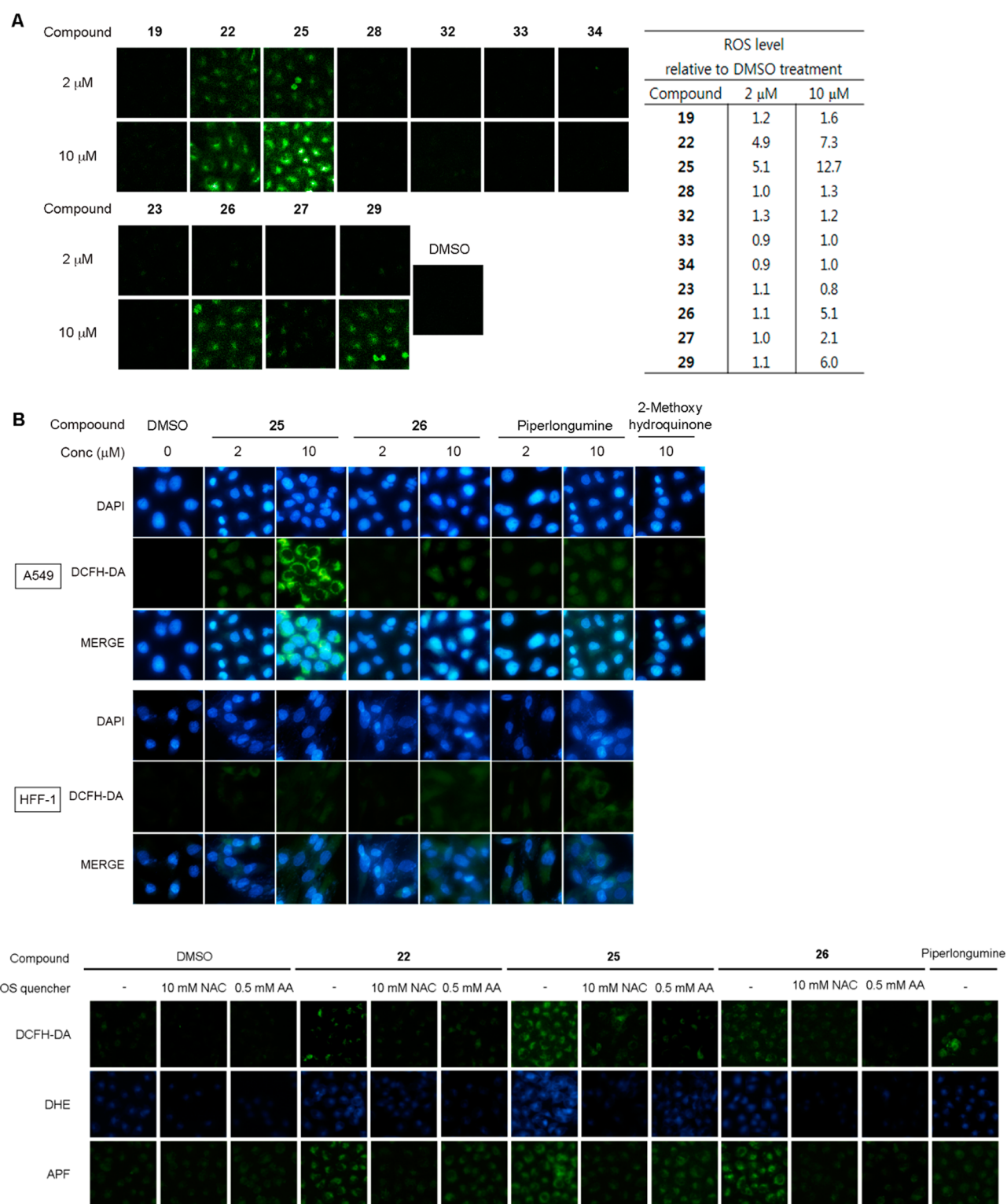
Figure 2. Compound **22** and its cytotoxic analogues showed evident induction of intracellular ROS in A549 lung cancer cells. Cells were treated with the indicated concentrations of compounds for 3 h before staining with 10 μM DCF-DA for 30 min and then fixing with 4% formaldehyde for 20 min. (A) Compound **22** strongly generated ROS, and its hydroquinone form, **25**, does so to a greater extent. A moderate ROS level was observed from **26**, **27**, and **29**, whereas almost no ROS induction was detected from the rest of the compounds. Fluorescence signal was detected and quantified using an Operetta high-content imaging system. (B) Compounds **25** and **26** showed more prominent ROS induction in A549 cancer cells than that in HFF-1 fibroblasts. Selective ROS generation was particularly evident from **25**. In addition, only marginal ROS levels were observed from 2-methoxyhydroquinone in A549 cells. Fluorescence was detected using a fluorescence microscope. (C) Similar experiments were done in A549 cells using three different ROS probes (DCF-DA, DHE, APF) with pretreatment with 10 mM NAC or 0.5 mM AA. Compound **25** increased ROS levels most significantly in A549 cells, whereas **22**, **26**, and piperlongumine increased ROS levels to a lesser extent. Pretreatment with NAC or AA greatly diminished ROS generation.

Figure 3. Both **25** and **26** activated Akt and multiple MAPKs in A549 and HCT-116 cells in a ROS-dependent manner. (A) Treatment with **25** or **26** for 3 h enhanced phosphorylation of Akt, JNK, p38, and ERK1/2 in A549 and HCT-116 cells in a dose-d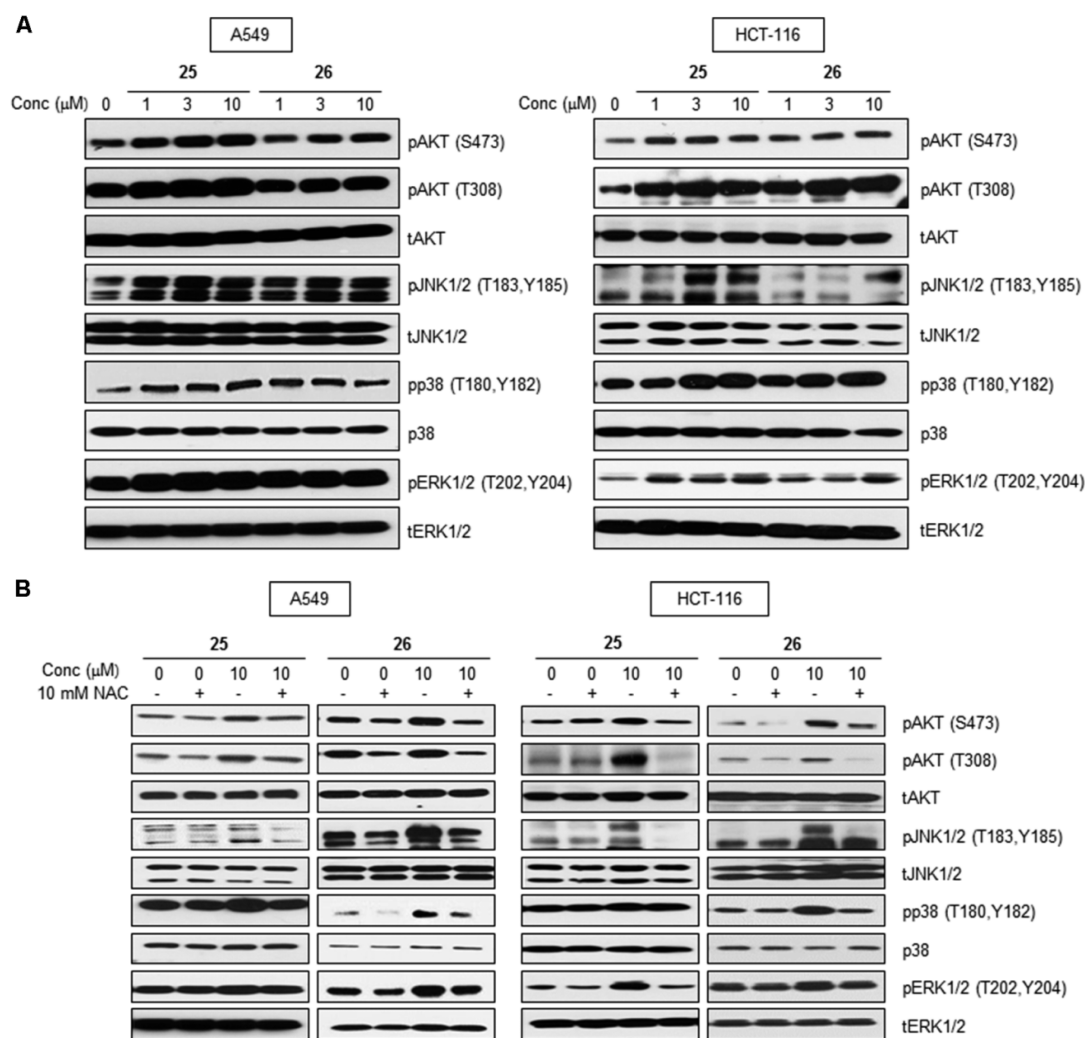ependent manner. (B) A549 and HCT-116 cells were pretreated with 10 mM NAC for 2 h prior to treatment with **25** or **26** at 10 μM for 3 h. NAC significantly attenuated the activation of Akt, JNK, p38, and ERK1/2, indicating that the compounds induced ROS-mediated activation of Akt, JNK, p38, and ERK1/2.

HFF-1 cells might be associated with its selective ROS production in A549 cells. In addition, 2-methoxyhydroquinone, which showed no cytotoxicity (Table 1), barely induced ROS in cells, indicating that not only hydroquinone but also the naturally occurring 17-carbon chain plays a major role in escalating intracellular ROS levels.

We then compared **22**, **25**, and **26** with piperlongumine with regard to their capability of inducing ROS in A549 cells. Besides DCF-DA, which detects a broad range of ROS including hydrogen peroxide, hydroxyl radical, and peroxy radicals, we employed two other ROS sensors that probe more specific ROS in cells.[19] APF (3′-(*p*-aminophenyl) fluorescein) mainly senses hydroxy radical, whereas dihydroethidium (DHE) selectively detects superoxide anion in cells. Fluorescence imaging with the three different ROS probes showed consistent results for the ROS inducers. Notably, the level of ROS generated by **25** outcompeted that induced by piperlongumine, whereas **22**, **26**, and piperlongumine showed similar levels of ROS induction (Figure 2C). When we pretreated cells with either 10 mM *N*-acetyl cysteine (NAC) or 0.5 mM ascorbic acid (AA) as an antioxidant prior to

treatment with the compounds (10 μM), ROS generation was greatly attenuated.

We also found that compounds with a 12-carbon chain (e.g., **26**) showed better cytotoxicity but released ROS to a lesser extent than those with a 17-carbon chain (e.g., **25**). In fact, the discrepancy between ROS generation and cytotoxicity has been reported by others.[14,20] For example, the cytotoxicity of piperlongumine analogues is well-correlated with the ability to deplete cellular glutathione (GSH) rather than the ability to induce ROS in cells.[14] Thus, we compared the ability of **25**, **26**, and piperlongumine to deplete intracellular GSH in A549 cells (Figure S1, Supporting Information). Compound **25** sparingly affected the total GSH level and marginally reduced the reduced GSH level, whereas it slightly increased the level of oxidized glutathione (GSSG). This suggests that the high level of ROS induced by **25** caused oxidation of intracellular GSH into GSSG. On the other hand, consistent with previous reports,[13,14,20] piperlongumine significantly suppressed the level of total GSH. Compound **26** depleted the total GSH level more significantly than piperlongumine, which might be associated with its stronger cytotoxicity. Thus, unlike **25**, whose mechanism of action seems to be mainly attributed to ROS
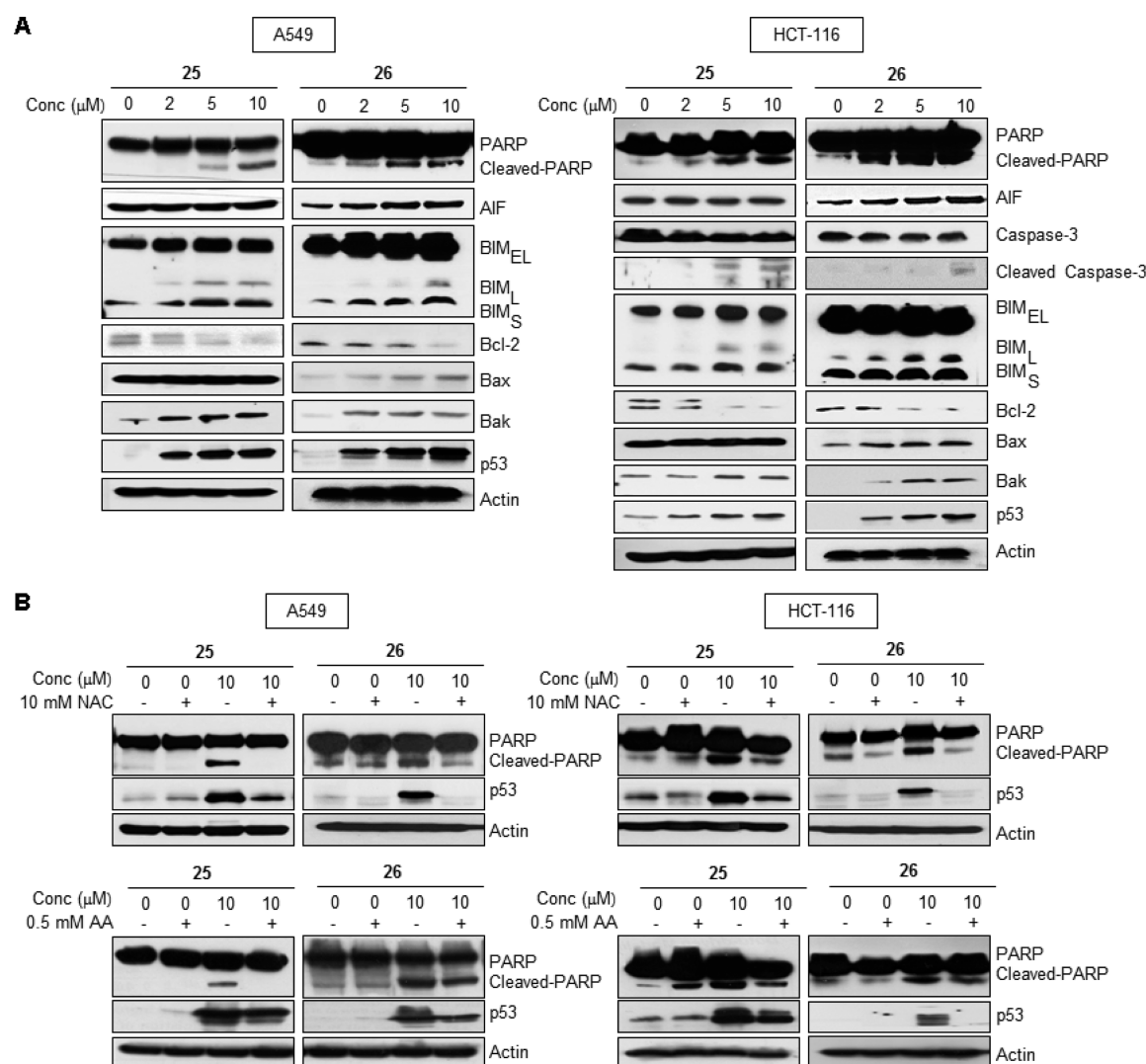
Figure 4. Both **25** and **26** induced apoptosis in A549 and HCT-116 cells through generation of ROS. (A) Western blot analysis showed that treatment with **25** or **26** for 48 h caused apoptosis in A549 and HCT-116 cells in a dose-dependent manner. The levels of apoptotic markers (PARP, AIF, BIM, BAX, BAK, and p53) were increased, whereas antiapoptotic marker Bcl-2 was downregulated. (B) Pretreatment with 10 mM NAC or 0.5 mM AA prior to **25** or **26** at 10 μM blocked the generation of PARP cleavage and p53 in A549 and HCT-116 cells, indicating that **25** and **26** induced apoptosis through ROS generation.

generation, piperlongumine and **26** might have mechanisms for perturbing GSH homeostasis as well, contributing to apoptosis.[21]

It has been reported that in response to ROS, MAPK pathways such as JNK, p38, and ERK1/2 are activated, ultimately leading to apoptosis.[22−25] As **25** and **26** induced prominent ROS generation, we investigated whether they upregulated MAPK pathways. Western blot analysis using A549 and HCT-116 cancer cells showed that treatment with **25** or **26** for 3 h increased the phosphorylation of JNK1/2, p38, and ERK1/2 in dose-dependent manner (Figure 3A). We also observed that phosphorylation of Akt was increased in a similar fashion in both A549 and HCT-116 cells. To confirm that the Akt/MAPK pathways were activated by ROS generation, cells were pretreated with 10 mM NAC prior to treatment with 10 μM **25** or **26**, and then the phospho-levels were examined. NAC negated the increase of both phospho-Akt and phospho-MAPKs, confirming that **25** and **26** activated Akt and MAPK pathways in a ROS-dependent manner (Figure 3B). Because the antioxidant removed the basal level of ROS, treatment with

NAC itself also downregulated the basal phospho-levels of Akt, JNK, p38, and ERK1/2. Activation of these kinases is usually associated with cell proliferation and survival. However, it has also been reported that increased MAPK and Akt phosphorylation sensitize cells to oxidative stress, thereby inducing apoptosis.[26−29] Thus, the increased ROS levels and the enhanced kinase activity induced by the compounds might be synergistically exerted in both of these cancer cell lines, inducing apoptosis.

Then, we examined apoptosis in A549 and HCT-116 cells following treatment with the compounds for 48 h. Western blot analysis showed that both **25** and **26** increased the levels of apoptotic markers, including cleaved PARP, cleaved caspase-3, BIM, BAK, and p53, and decreased antiapoptotic marker Bcl-2 in a dose-dependent manner (Figure 4A). Likewise, pretreatment with 10 mM NAC or 0.5 mM AA attenuated the escalation of p53 and cleaved PARP (Figure 4B), indicating that **25** and **26** induced apoptosis through generation of ROS. We also confirmed apoptosis from FACS analysis of A549 and
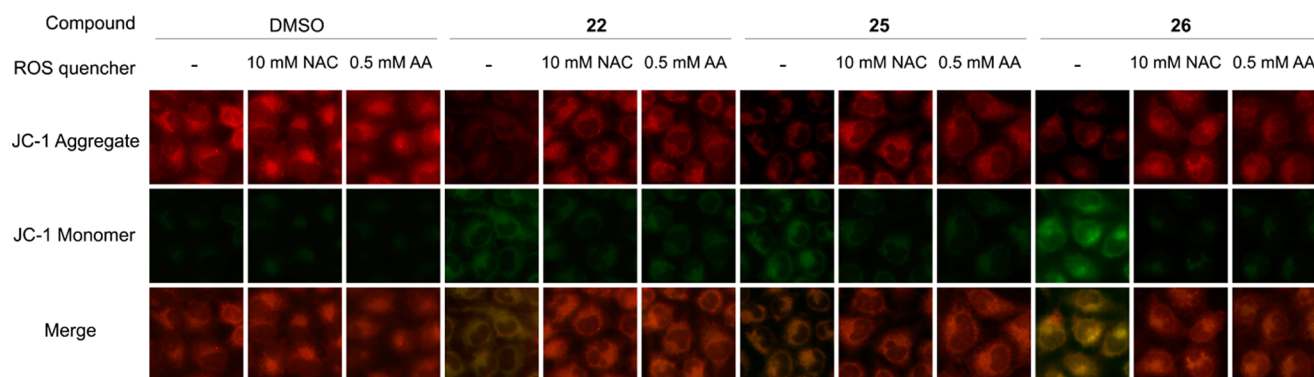
Figure 5. Compounds **22**, **25**, and **26** disrupted mitochondrial membrane integrity in A549 cells through generation of ROS. A549 cells were treated with 10 μM **22**, **25**, or **26** for 24 h before JC-1 staining. Compound **26** greatly reduced mitochondrial membrane potential, whereas **22** and **25** reduced it to a lesser extent. Pretreatment with 10 mM NAC or 0.5 mM AA significantly negated the effect of the compounds, indicating that the three compounds induced a loss of mitochondrial membrane integrity in A549 cells through generation of ROS.
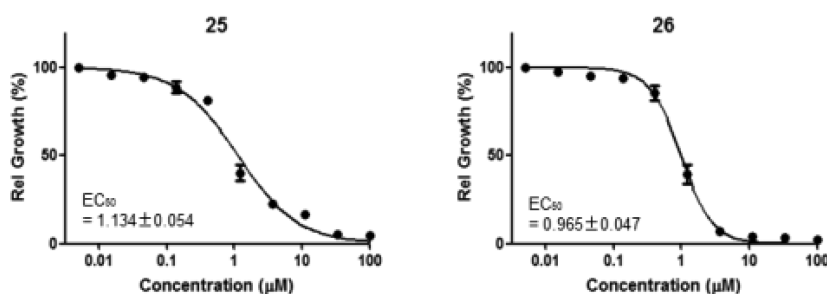

Figure 6. Compounds **25** and **26** potently blocked proliferation of p53-deficient H1299 lung cancer cells.

HCT-116 cells following treatment with 10 μM **26** for 48 h (Figure S2, Supporting Information).

In order to assess whether observed apoptosis was mediated through mitochondria, we monitored mitochondrial outer membrane potential. JC-1 (5,5′,6,6′-tetrachloro-1,1′,3,3′-tetraethylbenzimidazolocarbocyanine iodide) is a mitochondrial potential-sensitive fluorometric probe.[30] It reversibly changes from a red aggregate to a green monomer as the membrane potential decreases due to apoptosis. Imaging analysis using JC-1 showed that 24 h treatment with **25** or **26** at 10 μM increased the green monomeric form of JC-1 in A549 cells (Figure 5), indicating mitochondrial membrane depolarization and apoptosis. Moreover, **26** generated a higher JC-1 green fluorescence signal than **25**, which was consistent with the higher antiproliferative activity of **26** measured with the MTT assay (Table 1). Cotreatment with either 10 mM NAC or 0.5 mM AA attenuated the loss of mitochondrial membrane potential, indicating that disruption of mitochondrial membrane integrity was dependent on ROS generation.

We then performed a soft agar assay using A549 cells with treatment of **25**, **26**, and piperlongumine at 10 μM for 10 days (Figure S3, Supporting Information). Piperlongumine and **25** significantly decreased the colony size, whereas **26** reduced the size more significantly. This result showed that **25** and **26** were effective in blocking anchorage-independent A549 cell growth *in vitro*.

Both JC-1 staining and western blot analysis indicated that **25** and **26** are potent inducers of apoptosis. As both compounds enhanced p53 levels (Figure 4), they induced p53-mediated apoptosis. We examined the cytotoxicity of **25** and **26** against p53-deficient H1299 lung cancer cells as well. Interestingly, both compounds showed potent activities (ca. 1

μM EC$_{50}$'s) against H1299 cells, comparable to the activity against p53$^{+/+}$ A549 lung cancer cells (Figure 6). This result suggests that our compounds induce cell death in a p53-independent manner as well and demonstrates their broad spectrum of anticancer effects.

Herein, we described the synthesis of the 17-carbon chain-tethered quinone part (**22**) of the proposed structure of natural product irisferin A and its derivatives. There is no report yet about **22** and its derivatives as ROS inducers. Thus, we report that they are novel ROS inducers. We found that **22** itself is a strong ROS inducer and kills cancer cells with good potency and selectivity. Among our synthetic analogues of **22**, **25** and **26** induced ROS generation and exhibited the highest cytotoxicity against cancer cells. Compound **25**, the hydroquinone form of **22**, was the most potent ROS inducer and selectively produced high levels of ROS in cancer cells. It turned out to be superior to piperlongumine in terms of ROS induction capability and antiproliferative activity and was selective against cancer cells over noncancerous cells. Compound **26**, bearing a shorter 12-carbon chain, induced lower levels of ROS compared with those from **25**, but it exhibited higher antiproliferative activities against A549 and HCT-116 cells, indicating that, aside from ROS generation, there might be another mechanism for the cytotoxicity elicited by **26**.

It is well-documented that (hydro)quinones produce ROS, thereby damaging cancer cells. Interestingly, our study revealed that the naturally occurring 17-carbon chain moiety attached to the (hydro)quinone backbone also plays a critical role in generating ROS in cancer cells and confers selectivity over noncancerous cells. To the best of our knowledge, this is the first report demonstrating that the long hydrocarbon chain on

(hydro)quinone is crucial for ROS generation and cytotoxicity in cancer cells. It is also worth mentioning that our ROS inducers showed strong inhibitory activities against vemurafenib-resistant SK-Mel2 melanoma cells and p53-null H1299 lung cancer cells as well. Our study demonstrates that further tuning of our compounds could lead to decent small molecule agents that effectively and selectively target various cancers.

CONCLUSIONS

Here, we synthesized the 17-carbon chain-tethered quinone moiety (**22**) within the proposed structure of natural product irisferin A and its derivatives. For the first time, we found them to be novel ROS inducers and report that the naturally occurring 17-carbon chain is critical for ROS generation and selective cytotoxicity toward cancer cells over noncancerous cells. We found that **25**, the reduced form of **22**, generated an exceptionally high level of intracellular ROS and potently killed cancer cells (EC_{50} = ca. 1.3−2.6 μM). Interestingly, another analogue, **26**, bearing a shorter 12-carbon chain showed a higher cytotoxicity (EC_{50} = ca. 0.8−1.6 μM) but generated a lower level of ROS than that with **25**, which suggest that another mode of action might be involved in its potent cytotoxicity. Both **25** and **26** activated Akt and multiple MAPK pathways in a ROS-dependent fashion, thereby inducing apoptosis. Both compounds showed stronger antiproliferative activity than piperlongumine against four cancer cell lines (A549, A375, SK-Mel2, and HCT116 cells). In particular, compound **25** turned out to be superior to piperlongumine not only in terms of antiproliferative activity against cancer cells but also selectivity over noncancerous cells (HFF-1, MCF10A, and HaCaT cells). Their potent antiproliferative activities against various cancer cells, including vemurafenib-resistant SK-Mel2 melanoma cells and p53-null H1299 lung cancer cells, also demonstrate the broad therapeutic potential of **25** and **26** as anticancer agents.

EXPERIMENTAL SECTION

Chemical Synthesis. *General.* Reactions were monitored by TLC using 0.25 mm Merck precoated silica gel plates (60F254). Reaction progress was monitored by TLC analysis using a UV lamp or ninhydrin/*p*-anisaldehyde stain for detection purposes. Commercially available reagents were used without further purification. All solvents were purified by standard techniques. Purification of reaction products was carried out by silica gel column chromatography using Kieselgel 60 Art. 9385 (230−400 mesh). The purity of all compounds was over 95% and was analyzed using a Waters LC/MS system (Waters 2998 photodiode array detector, Waters 3100 mass detector, Waters SFO system fluidics organizer, Waters 2545 binary gradient module, Waters reagent manager, and Waters 2767 sample manager) using a SunFireTM C18 column (4.6 × 50 mm, 5 μm particle size). The solvent gradient was 60% (or 95%) A at 0 min and 1% A at 5 min. Solvent A was 0.035% TFA in H_2O; solvent B was 0.035% TFA in MeOH. The flow rate was 3.0 (or 2.5) mL/min. ^{1}H and ^{13}C NMR spectra were obtained using a Bruker 400 MHz FT-NMR (400 MHz for ^{1}H and 100 MHz for ^{13}C) spectrometer. Chemical shifts are reported relative to CHCl$_3$ (δ = 7.26) for ^{1}H NMR and CHCl$_3$ (δ = 77.0) for ^{13}C NMR. Standard abbreviations are used to denote signal multiplicities. Infrared spectra were measured on an FT-IR Nicolet iS10 spectrometer. Samples were recorded neat or as KBr optics. High-resolution mass spectra (HRMS) were recorded on a Q-TOF mass spectrometer.

(Z)-3-(Heptadec-10-en-1-yl)-5-methoxyphenol (19). To a suspension of 60% NaH (963 mg, 24 mmol) in DMF (20 mL) was added a solution of ethanethiol (1.86 mL, 24.34 mmol). The mixture was stirred for 5 min, treated with a solution of **16** (2 g, 5.35 mmol) in DMF (20 mL), and refluxed overnight. After being cooled to room temperature, the solution was acidified with 2 N HCl and extracted with ether. The organic layer was washed with brine solution, dried over MgSO$_4$, and concentrated under vacuum. The resulting crude product was purified by silica gel column chromatography (EtOAc/hexane 1:4) to afford compound **19** (1.8 g, 94%) as a pale yellow liquid. R_f = 0.2 (20% EtOAc/hexane); IR (neat, KBr): 3405, 2926, 2855, 1615, 1597, 1458, 1147 cm^{-1}; ^{1}H NMR (400 MHz, CDCl$_3$): 6.34 (d, J = 2.6 Hz, 1H), 6.29 (t, J = 2.6 Hz, 2H), 5.36−5.34 (m, 2H), 3.78 (s, 3H), 2.54 (t, J = 7.6 Hz, 2H), 2.05−1.96 (m, 4H), 1.64−1.56 (m, 2H), 1.33−1.28 (m, 20H), 0.88 (t, J = 6.7 Hz, 3H); ^{13}C NMR (100 MHz, CDCl$_3$): δ 160.6, 156.4, 145.7, 129.9, 129.8, 108.0, 106.7, 98.7, 55.2, 36.0, 32.5, 31.7, 31.1, 29.7(2), 29.6, 29.5(2), 29.3(2), 28.9, 27.2, 22.6, 14.1; HRMS (ESI): calcd. for C$_{24}$H$_{40}$O$_2$Na [M + Na]$^+$, 383.2926; found, 383.2918.

(Z)-2-(Heptadec-10-en-1-yl)-6-methoxycyclohexa-2,5-diene-1,4-dione (22). Into a stirred solution of **19** (220 mg) and salcomine (25 mg) in DMF (5 mL) was bubbled oxygen at room temperature for 24 h. The mixture was diluted with water and extracted with ether. The organic layer was washed with brine solution, dried over MgSO$_4$, and concentrated under vacuum. The resulting crude product was purified by silica gel column chromatography (EtOAc/hexane 1:20) to afford **22** (95 mg, 42%) as brown liquid. R_f = 0.5 (20% EtOAc/hexane); IR (neat, KBr): 2950, 2854, 1680, 1652, 1601, 1485 cm^{-1}; ^{1}H NMR (400 MHz, CDCl$_3$): 6.47 (d, J = 2.2 Hz, 1H); 5.86 (d, J = 2.2 Hz, 1H); 5.34 (t, J = 5.5 Hz, 2H); 3.81 (s, 3H); 2.42 (t, J = 8.3 Hz, 2H); 2.00 (q, J = 6.3 Hz, 4H); 1.53−1.45 (m, 2H); 1.32−1.21 (m, 20H), 0.88 (t, J = 7.0 Hz, 3H); ^{13}C NMR (100 MHz, CDCl$_3$): δ 187.5, 181.9, 158.7, 147.4, 132.7, 129.7, 129.6, 106.9, 56.1, 31.6, 29.6, 29.4, 29.3(3), 29.2, 29.1, 28.8, 28.5, 27.6, 27.1, 27.0, 22.5, 13.9; HRMS (ESI): calcd. for C$_{24}$H$_{38}$O$_3$Na [M + Na]$^+$, 397.2719; found, 397.2715.

(Z)-2-(Dodec-5-en-1-yl)-6-methoxycyclohexa-2,5-diene-1,4-dione (23). Into a stirred solution of **20** (100 mg) and salcomine (15 mg) in DMF (3 mL) was bubbled oxygen at room temperature for 24 h. The mixture was diluted with water and extracted with ether. The organic layer was washed with brine, dried over MgSO$_4$, and concentrated under vacuum. The resulting crude product was purified by silica gel column chromatography (EtOAc/hexane 1:20) to afford **23** (41 mg, 41%) as a yellow liquid. R_f = 0.5 (20% EtOAc/hexane); IR (neat, KBr): 2926, 2853, 1660, 1602, 1458, 1230 cm^{-1}; ^{1}H NMR (400 MHz, CDCl$_3$): 6.47 (m, 1H), 5.86 (d, J = 2.3 Hz, 1H), 5.42−5.27 (m, 2H), 3.81 (s, 3H), 2.43 (t, J = 8.5 Hz, 2H), 2.08−1.93 (m, 4H), 1.55−1.46 (m, 2H), 1.44−1.36 (m, 2H), 1.34−1.21 (m, 8H), 0.87 (t, J = 7.0 Hz, 3H); ^{13}C NMR (100 MHz, CDCl$_3$): δ 187.5, 182.0, 158.7, 147.3, 132.8, 130.5, 128.9, 107.0, 56.2, 31.7, 29.6, 29.2, 28.9, 28.5, 27.2(2), 26.7, 22.5, 14.0; HRMS (ESI): calcd. for C$_{19}$H$_{28}$O$_3$Na [M + Na]$^+$, 327.1937; found, 327.1936.

(Z)-2-(Heptadec-10-en-1-yl)-6-methoxybenzene-1,4-diol (25). To a stirred solution of **22** (90 mg, 0.24 mmol) in THF/MeOH/H$_2$O (4:3:3, 10 mL) was added Na$_2$S$_2$O$_4$ (170 mg, 0.96 mmol) at room temperature. The reaction mixture was stirred for 24 h, condensed under vacuum, and extracted with EtOAc. The organic layer was washed with water and brine solution, dried over MgSO$_4$, and concentrated under vacuum. The residue was purified by silica gel column chromatography (EtOAc/hexane 1:15) to afford **25** (56 mg, 62%) as a yellow solid. R_f = 0.4 (20% EtOAc/hexane); IR (neat, KBr): 3551, 3325, 1649, 1601, 1458 cm^{-1}; ^{1}H NMR (400 MHz, CDCl$_3$): 6.31 (d, J = 2.7 Hz, 1H), 6.20 (d, J = 2.7 Hz, 1H), 5.35 (t, J = 4.6 Hz, 2H), 5.22 (brs, 1H), 3.84 (s, 3H), 2.56 (t, J = 7.6 Hz, 2H), 2.05−1.99 (m, 4H), 1.61−1.53 (m, 2H), 1.31−1.24 (m, 20H), 0.88 (t, J = 7.0 Hz, 3H); ^{13}C NMR (100 MHz, CDCl$_3$): δ 148.3, 146.7, 137.3, 129.9, 129.8, 129.0, 107.9, 97.0, 55.5, 31.7, 29.7(4), 29.6, 29.5(4), 29.3, 28.9, 27.2, 22.6, 14.1; HRMS (ESI): calcd. for C$_{24}$H$_{40}$O$_3$Na [M + Na]$^+$, 399.2875; found, 399.2862.

(Z)-2-(Dodec-5-en-1-yl)-6-methoxybenzene-1,4-diol (26). To a stirred solution of **23** (50 mg, 0.16 mmol) in THF/MeOH/H$_2$O (4:3:3, 4 mL) was added Na$_2$S$_2$O$_4$ (25 mg, 0.48 mmol) at room temperature. The reaction mixture was stirred for 24 h, condensed under vacuum, and extracted with EtOAc. The organic layer was washed with water and brine solution, dried over MgSO$_4$, and

concentrated under vacuum. The residue was purified by silica gel column chromatography (EtOAc/hexane 1:15) to give **26** (30 mg, 61%) as a white solid. R_f = 0.4 (20% EtOAc/hexane); IR (neat, KBr): 3558, 3393, 2924, 2858, 1678, 1602, 1379, 1218 cm^{-1}; ^{1}H NMR (400 MHz, CDCl$_3$): 6.30 (d, J = 2.7 Hz, 1H), 6.22 (d, J = 2.7 Hz, 1H), 5.35 (t, J = 4.9 Hz, 2H), 5.26 (s, 1H), 3.82 (s, 3H), 2.58 (t, J = 7.8 Hz, 2H), 2.08−1.94 (m, 4H), 1.64−1.56 (m, 2H), 1.44−1.36 (m, 2H), 1.36−1.26 (m, 8H), 0.88 (t, J = 7.0 Hz, 3H); ^{13}C NMR (100 MHz, CDCl$_3$): δ 148.3, 146.7, 137.3, 130.1, 129.6, 128.8, 107.9, 97.1, 55.9, 31.7, 29.7, 29.5, 29.4, 29.3, 28.9, 27.2, 27.0, 22.6, 14.06; HRMS (ESI): calcd. for C$_{19}$H$_{30}$O$_3$Na [M + Na]$^+$, 329.2092; found, 329.2085.

(E)-2-(Dodec-5-en-1-yl)-6-methoxybenzene-1,4-diol (27). To a stirred solution of **24** (40 mg, 0.13 mmol) in THF/MeOH/H$_2$O (4:3:3, 4 mL) was added Na$_2$S$_2$O$_4$ (21 mg, 0.40 mmol) at room temperature. The reaction mixture was stirred for 24 h, condensed under vacuum, and extracted with EtOAc. The organic layer was washed with water and brine solution, dried over MgSO$_4$, and concentrated under vacuum. The residue was purified by silica gel column chromatography (EtOAc/hexane 1:15) to give **27** (24 mg, 61%) as an off-white solid. R_f = 0.4 (20% EtOAc/hexane); IR (neat, KBr): 3557, 3390, 2925, 2858, 1678, 1600, 1379, 1218 cm^{-1}; ^{1}H NMR (400 MHz, CDCl$_3$): 6.30 (d, J = 2.7 Hz, 1H), 6.20 (d, J = 2.7 Hz, 1H), 5.40−5.34 (m, 2H), 5.22 (s, 1H), 3.84 (s, 3H), 2.60−2.55 (m, 2H), 2.08−1.94 (m, 4H), 1.65−1.55 (m, 2H), 1.36−1.20 (m, 10H), 0.88 (t, J = 6.6 Hz, 3H); ^{13}C NMR (100 MHz, CDCl$_3$): δ 148.2, 146.7, 137.4, 130.5, 130.1, 128.8, 107.9, 97.1, 55.9, 32.4, 31.7, 29.7, 29.6, 29.5, 29.3, 28.9, 27.2, 22.6, 14.0; LCMS (ESI): 307 (M + H)$^+$.

(Z)-1-(Heptadec-10-en-1-yl)-2,3,5-trimethoxybenzene (28). A mixture of **25** (20 mg, 0.05 mmol), methyl iodide (0.1 mL), and K$_2$CO$_3$ (25 mg) in acetone (10 mL) was refluxed overnight. After being cooled to room temperature, the reaction mixture was diluted with water and extracted with EtOAc. The organic layer was washed with water and brine solution, dried over MgSO$_4$, and concentrated under vacuum. The residue was purified by silica gel column chromatography (EtOAc/hexane 1:30) to afford **28** (17 mg, 82%) as a yellow liquid. R_f = 0.2 (5% EtOAc/hexane); IR (neat, KBr): 2925, 2853, 1600, 1492, 1466, 1222, 1058 cm^{-1}; ^{1}H NMR (400 MHz, CDCl$_3$): 6.34 (d, J = 2.8 Hz, 1H), 6.28 (d, J = 2.8 Hz, 1H), 5.35 (t, J = 4.6 Hz, 2H), 3.83 (s, 3H), 3.77 (s, 3H), 3.75 (s, 3H), 2.58 (t, J = 7.9 Hz, 2H), 2.06−1.97 (m, 4H), 1.61−1.54 (m, 2H), 1.32−1.27 (m, 20H), 0.88 (t, J = 6.7 Hz, 3H); ^{13}C NMR (100 MHz, CDCl$_3$): δ 155.8, 153.2, 141.1, 136.9, 130.3, 129.9, 104.9, 97.6, 60.8, 55.6, 55.4, 32.6, 31.7, 30.8, 30.1, 29.7(2), 29.6, 29.5(3), 29.3, 28.9, 27.2, 22.6, 14.1; HRMS (ESI): calcd. for C$_{26}$H$_{44}$O$_3$Na [M + Na]$^+$, 427.3188; found, 427.3196.

2-Dodecyl-6-methoxybenzene-1,4-diol (29). To a stirred solution of **26** (20 mg, 0.06 mmol) in methanol was added Pd/C (2 mg) in one portion. The reaction mixture was stirred at room temperature for 2 h under hydrogen pressure and then filtered through a Celite pad. The filtrate was concentrated under vacuum to obtain **29** (18 mg, 98%) as a white solid. R_f = 0.35 (20% EtOAc/hexane); IR (neat, KBr): 3565, 3349, 2954, 2914, 2850, 1653, 1598, 1471, 1233 cm^{-1}; ^{1}H NMR (400 MHz, CDCl$_3$): 6.31 (d, J = 1.7 Hz, 1H), 6.22 (d, J = 1.7 Hz, 1H), 4.63 (brs, 1H), 3.84 (s, 3H), 2.57 (t, J = 7.9 Hz, 2H), 1.43−1.15 (m, 20H), 0.89 (t, J = 7.0 Hz, 3H); ^{13}C NMR (100 MHz, CDCl$_3$): δ 148.2, 146.7, 137.4, 129.0, 107.9, 97.0, 56.0, 31.9, 29.7, 29.6(3), 29.5, 29.3(4), 22.7, 14.1; HRMS (ESI): calcd. for C$_{19}$H$_{32}$O$_3$Na [M + Na]$^+$, 331.2249; found, 331.2226.

(Z)-3-(Heptadec-10-en-1-yl)-2,5-dimethoxycyclohexa-2,5-diene-1,4-dione (32). To a stirred solution of **31** (100 mg, 0.22 mmol) and tetrakis(triphenylphosphine)palladium (5 mg) in CH$_3$OH/THF (1:1, 10 mL) under argon was added a 2 N Na$_2$CO$_3$ solution (0.5 mL). The mixture was stirred for 10 min at 90 °C, concentrated under vacuum, and partitioned between EtOAc and water. The EtOAc layer was washed with brine solution, dried over MgSO$_4$, and concentrated under vacuum. The residue was purified by silica gel column chromatography (EtOAc/hexane 1:20) to afford **32** (58 mg, 65%) as a liquid. R_f = 0.5 (20% EtOAc/hexane); IR (neat, KBr): 2924, 2853, 1657, 1598, 1384, 1048 cm^{-1}; ^{1}H NMR (400 MHz, CDCl$_3$): δ 5.72 (s, 1H), 5.38−5.29 (m, 2H), 4.04 (s, 3H), 3.79 (s, 3H), 2.42 (t, J = 7.3

Hz, 2H), 2.03−1.96 (m, 4H), 1.41−1.26 (m, 24H), 0.87 (t, J = 6.7 Hz, 3H); ^{13}C NMR (100 MHz, CDCl$_3$): δ 183.6, 182.4, 158.7, 155.8, 130.7, 129.9, 129.8, 105.3, 61.3, 56.3, 31.7, 29.7(2), 29.6(2), 29.5, 29.4, 29.3(2), 28.9, 28.6, 27.2, 23.0, 22.6, 14.1; HRMS (ESI): calcd. for C$_{25}$H$_{40}$O$_4$Na [M + Na]$^+$, 427.2824; found, 427.2815.

(Z)-3-(Heptadec-10-en-1-yl)-2,5-dimethoxybenzene-1,4-diol (33). To a stirred solution of **32** (30 mg, 0.07 mmol) in THF/MeOH/H$_2$O (4:3:3, 2 mL) was added Na$_2$S$_2$O$_4$ (50 mg, 0.96 mmol) at room temperature. The reaction mixture was stirred for 24 h, condensed under vacuum, and extracted with EtOAc. The organic layer was washed with water and brine solution, dried over MgSO$_4$, and concentrated under vacuum. The residue was purified by silica gel column chromatography (EtOAc/hexane 1:15) to give **33** (12 mg, 51%) as a yellow liquid. R_f = 0.5 (20% EtOAc/hexane); IR (neat, KBr): 3553, 3370, 1608, 1482, 1452 cm^{-1}; ^{1}H NMR (400 MHz, CDCl$_3$): 6.43 (s, 1H), 5.34 (t, J = 4.7 Hz, 2H), 5.26 (s, 1H), 5.23 (s, 1H), 3.82 (s, 3H), 3.74 (s, 3H), 2.64 (t, J = 7.9 Hz, 2H), 2.02−1.97 (m, 4H), 1.63−1.55 (m, 2H), 1.43−1.28 (m, 20H), 0.88 (t, J = 7.0 Hz, 3H); ^{13}C NMR (100 MHz, CDCl$_3$): 158.8, 155.9, 138.9, 137.1, 130.7, 129.9, 105.4, 96.8, 61.7, 56.1, 31.8, 29.9, 29.7, 29.6, 29.5(3), 29.4(4), 28.7, 27.2, 22.6, 14.1.

(Z)-3-(Heptadec-10-en-1-yl)-2-hydroxy-5-methoxycyclohexa-2,5-diene-1,4-dione (34). To a stirred solution of **32** (50 mg) in CH$_2$Cl$_2$ (5 mL) was added a catalytic amount of HClO$_4$ (60%) at room temperature. The reaction mixture was stirred for 12 h, washed with NaHCO$_3$ solution and brine solution, dried over MgSO$_4$, and concentrated under vacuum. The residue was purified by silica gel column chromatography (EtOAc/hexane 1:5) to afford **34** (40 mg, 83%) as yellow solid. R_f = 0.2 (20% EtOAc/hexane); IR (neat, KBr): 3344, 2921, 2851, 1660, 1596, 1384, 1202 cm^{-1}; ^{1}H NMR (400 MHz, CDCl$_3$): 7.21 (brs, 1H), 5.83 (s, 1H), 5.34 (t, J = 4.9 Hz, 2H), 3.85 (s, 3H), 2.43 (t, J = 7.4 Hz, 2H), 2.04−1.98 (m, 4H), 1.51−1.40 (m, 2H), 1.27−1.24 (m, 20H), 0.88 (t, J = 6.7 Hz, 3H); ^{13}C NMR (100 MHz, CDCl$_3$): δ 182.7, 181.6, 161.1, 151.5, 130.3, 129.8, 119.2, 102.1, 56.7, 32.6, 31.7, 31.5, 29.7(2), 29.5(2), 29.4, 29.3, 28.9, 28.0, 27.2, 22.6(2), 14.1; HRMS (ESI): calcd. for C$_{24}$H$_{38}$O$_4$Na [M + Na]$^+$, 413.2668; found, 413.2656.

Biological Experiments. *Cell Proliferation Assay (MTT Assay).* Cells (5000−30000 cells/well) were seeded in a 96-well plate. After 18−24 h, cells were treated with the serially diluted (3-fold, 12 point) compounds and were incubated at 37 °C in a 5% CO$_2$ atmosphere for 72 h. Cells were then subjected to MTT solutions (Promega) following the manufacturer's procedure. The optical density at 570 nm of each well was detected using a plate reader (Envision, PerkinElmer). The data was analyzed using Prism 5 software (GraphPad).

Western Blot Analysis. Cells were seed at a density of 6 × 10^5 cells/well in a 60 mm dish and incubated overnight. Cells were treated with the compounds at 37 °C in a 5% CO$_2$ atmosphere, washed twice with cold PBS, and then scraped with RIPA buffer. The resulting cell lysates were centrifuged at 15 000 rpm for 20 min. Total protein concentration was determined by BCA assay (Pierce). A total of 25−50 μg of the lysate was used for western blot analysis. Proteins separated by SDS-PAGE were electrophoretically transferred to methanol-activated PVDF membranes. After blocking in 1× TBS/T containing 5% nonfat dry milk for 1 h, membranes were incubated with primary antibodies overnight at 4 °C. After washing, the blots were incubated with 1:2000 dilutions of horseradish peroxidase-conjugated secondary antibodies (Santa Cruz Biotechnology) for 1 h at room temperature. After washing, the immune-reactive proteins were visualized using ECL reagents.

Measurement of Intracellular ROS Levels. Cells were seeded at 1 × 10^6 cells/well in a 12-well plate onto cover glass and incubated for 18−24 h. Cells were then treated with the compounds for the indicated periods of time and dosages, treated with 10 μM DCF-DA (Sigma), DHE (Sigma), or APF (Invitrogen) for 30 min, and fixed with 4% formaldehyde for 20 min. The cells were washed with PBS twice, and fluorescence was detected via fluorescence microscopy (Nikon). For a similar assay using a high-content cellular imaging system, cells were seeded at 1 × 10^4 cells/well in a black 96-well plate and incubated for 18−24 h. Cells were then treated with the compounds for 3 h, treated

with 10 μM DCF-DA for 30 min, and fixed with 4% formaldehyde for 20 min. The cells were washed with PBS twice, and fluorescence was detected via Operetta (PerkinElmer).

Detection of Mitochondrial Membrane Potential. Cells were seeded at 5×10^5 cells/well in a 24-well plate onto cover glass. After 18−24 h, the cells were treated with 10 mM compounds for 24 h. Cells were then treated with 10 μM JC-1 (Sigma) for 30 min and washed with PBS twice. Fluorescence was detected via fluorescence microscopy (Nikon).

■ ASSOCIATED CONTENT

Ⓢ Supporting Information

Protocols for biochemical and cellular assays. Figure S1: Measurement of cellular GSH and GSSG levels in A549 cells following compound treatment for 4 h. Figure S2: FACS analysis of apoptosis in A549 and HCT-116 cells after treatment of **26** for 48 h. Figure S3: Soft agar assay using A549 cells. This material is available free of charge via the Internet at http://pubs.acs.org.

■ AUTHOR INFORMATION

Corresponding Authors
*(W.H.) E-mail: whur@kist.re.kr. Phone: +82-2-958-5193.
*(T.S.) E-mail: tbsim@kist.re.kr, tbsim@korea.ac.kr. Phone: +82-2-958-6437.

Author Contributions
[§]Y.H. and S.S. contributed equally to this work.

Notes
The authors declare no competing financial interest.

■ ACKNOWLEDGMENTS

■ ABBREVIATIONS USED

ROS, reactive oxygen species; NAC, *N*-acetyl-cysteine; AA, ascorbic acid; SAR, structure−activity relationship; FACS, fluorescence-activated cell sorting; DCF-DA, 2′,7′-dichloro-fluorescein diacetate; APF, 3′-(*p*-aminophenyl) fluorescein; DHE, dihydroethidium; MTT, 3-(4,5-dimethylthiazol-2-yl)-2,5-diphenyl tetrazolium bromide; JC-1, 5,5′,6,6′-tetrachloro-1,1′,3,3′-tetraethylbenzimidazolocarbocyanine iodide; EC_{50}, effective concentration 50%; GSH, glutathione; NBS, *N*-bromosuccinimide; TLC, thin-layer chromatography; PCC, pyridinium chlorochromate; DMF, *N,N*-dimethylformamide; MBT, mercaptobenzothiazole

■ REFERENCES

(1) Mann, J. Natural products in cancer chemotherapy: past, present and future. *Nat. Rev. Cancer* **2002**, *2*, 143−148.

(2) Newman, D. J.; Cragg, G. M. Natural products as sources of new drugs over the 30 years from 1981 to 2010. *J. Nat. Prod* **2012**, *75*, 311−335.

(3) Choi, S. W.; Choi, C. H.; Ryu, S. Y.; Kim, Y. S.; Cha, M. R.; Kim, M. J.; Jeon, J. H.; Kim, Y. K. Anti-cancer substances containing resveratrol derivatives isolated from the seeds of *Iris pseudacorus*. Korea Patent 10-2012-0119693, October 31, 2012.

(4) Kim, Y. K.; Ahn, S. K.; Lee, M. Differential sensitivity of melanoma cell lines with differing B-Raf mutational status to the new oncogenic B-Raf kinase inhibitor UI-152. *Cancer Lett.* **2012**, *320*, 215−224.

(5) Keating, G. M. Vemurafenib: in unresectable or metastatic melanoma. *BioDrugs* **2012**, *26*, 325−334.

(6) Romano, E.; Pradervand, S.; Paillusson, A.; Weber, J.; Harshman, K.; Muehlethaler, K.; Speiser, D.; Peters, S.; Rimoldi, D.; Michielin, O. Identification of multiple mechanisms of resistance to vemurafenib in a patient with BRAFV600E-mutated cutaneous melanoma successfully rechallenged after progression. *Clin. Cancer Res.* **2013**, *19*, 5749−5757.

(7) Waris, G.; Ahsan, H. Reactive oxygen species: role in the development of cancer and various chronic conditions. *J. Carcinog.* **2006**, *5*, 14.

(8) Wu, W. S. The signaling mechanism of ROS in tumor progression. *Cancer Metastasis Rev.* **2006**, *25*, 695−705.

(9) Gorrini, C.; Harris, I. S.; Mak, T. W. Modulation of oxidative stress as an anticancer strategy. *Nat. Rev. Drug Discovery* **2013**, *12*, 931−947.

(10) Pelicano, H.; Carney, D.; Huang, P. ROS stress in cancer cells and therapeutic implications. *Drug Resist. Updates* **2004**, *7*, 97−110.

(11) Deavall, D. G.; Martin, E. A.; Horner, J. M.; Roberts, R. Drug-induced oxidative stress and toxicity. *J. Toxicol.* **2012**, *2012*, 645460.

(12) Trachootham, D.; Alexandre, J.; Huang, P. Targeting cancer cells by ROS-mediated mechanisms: a radical therapeutic approach? *Nat. Rev. Drug Discovery* **2009**, *8*, 579−591.

(13) Raj, L.; Ide, T.; Gurkar, A. U.; Foley, M.; Schenone, M.; Li, X.; Tolliday, N. J.; Golub, T. R.; Carr, S. A.; Shamji, A. F.; Stern, A. M.; Mandinova, A.; Schreiber, S. L.; Lee, S. W. Selective killing of cancer cells by a small molecule targeting the stress response to ROS. *Nature* **2011**, *475*, 231−234.

(14) Adams, D. J.; Dai, M.; Pellegrino, G.; Wagner, B. K.; Stern, A. M.; Shamji, A. F.; Schreiber, S. L. Synthesis, cellular evaluation, and mechanism of action of piperlongumine analogs. *Proc. Natl. Acad. Sci. U.S.A.* **2012**, *109*, 15115−15120.

(15) Shaw, A. T.; Winslow, M. M.; Magendantz, M.; Ouyang, C.; Dowdle, J.; Subramanian, A.; Lewis, T. A.; Maglathin, R. L.; Tolliday, N.; Jacks, T. Selective killing of K-ras mutant cancer cells by small molecule inducers of oxidative stress. *Proc. Natl. Acad. Sci. U.S.A.* **2011**, *108*, 8773−8778.

(16) Yuan, H.; Zhang, X.; Huang, X.; Lu, Y.; Tang, W.; Man, Y.; Wang, S.; Xi, J.; Li, J. NADPH oxidase 2-derived reactive oxygen species mediate FFAs-induced dysfunction and apoptosis of beta-cells via JNK, p38 MAPK and p53 pathways. *PLoS One* **2010**, *5*, e15726.

(17) Miki, H.; Uehara, N.; Kimura, A.; Sasaki, T.; Yuri, T.; Yoshizawa, K.; Tsubura, A. Resveratrol induces apoptosis via ROS-triggered autophagy in human colon cancer cells. *Int. J. Oncol.* **2012**, *40*, 1020−1028.

(18) Dharmaraja, A. T.; Jain, C.; Chakrapani, H. Substituent effects on reactive oxygen species (ROS) generation by hydroquinones. *J. Org. Chem.* **2014**, *79*, 9413−9417.

(19) Wardman, P. Fluorescent and luminescent probes for measurement of oxidative and nitrosative species in cells and tissues: progress, pitfalls, and prospects. *Free Radical Biol. Med.* **2007**, *43*, 995−1022.

(20) Zhu, C.; Hu, W.; Wu, H.; Hu, X. No evident dose−response relationship between cellular ROS level and its cytotoxicity—a paradoxical issue in ROS-based cancer therapy. *Sci. Rep.* **2014**, *4*, 5029.

(21) Anathy, V.; Roberson, E. C.; Guala, A. S.; Godburn, K. E.; Budd, R. C.; Janssen-Heininger, Y. M. Redox-based regulation of apoptosis: S-glutathionylation as a regulatory mechanism to control cell death. *Antioxid. Redox Signaling* **2012**, *16*, 496−505.

(22) Deng, Y. T.; Huang, H. C.; Lin, J. K. Rotenone induces apoptosis in MCF-7 human breast cancer cell-mediated ROS through JNK and p38 signaling. *Mol. Carcinog.* **2010**, *49*, 141−151.

(23) Bragado, P.; Armesilla, A.; Silva, A.; Porras, A. Apoptosis by cisplatin requires p53 mediated p38alpha MAPK activation through ROS generation. *Apoptosis* **2007**, *12*, 1733−1742.

(24) Wang, X.; Liu, J. Z.; Hu, J. X.; Wu, H.; Li, Y. L.; Chen, H. L.; Bai, H.; Hai, C. X. ROS-activated p38 MAPK/ERK−Akt cascade plays a central role in palmitic acid-stimulated hepatocyte proliferation. *Free Radical Biol. Med.* **2011**, *51*, 539−551.

(25) Mao, X.; Yu, C. R.; Li, W. H.; Li, W. X. Induction of apoptosis by shikonin through a ROS/JNK-mediated process in Bcr/Abl-positive chronic myelogenous leukemia (CML) cells. *Cell Res.* **2008**, *18*, 879−888.

(26) Dolado, I.; Nebreda, A. R. AKT and oxidative stress team up to kill cancer cells. *Cancer Cell* **2008**, *14*, 427−429.

(27) Esposito, F.; Chirico, G.; Montesano Gesualdi, N.; Posadas, I.; Ammendola, R.; Russo, T.; Cirino, G.; Cimino, F. Protein kinase B activation by reactive oxygen species is independent of tyrosine kinase receptor phosphorylation and requires SRC activity. *J. Biol. Chem.* **2003**, *278*, 20828−20834.

(28) Zhuang, S.; Schnellmann, R. G. H_2O_2-induced transactivation of EGF receptor requires Src and mediates ERK1/2, but not Akt, activation in renal cells. *Am. J. Physiol.: Renal Physiol.* **2004**, *286*, F858−F865.

(29) Ponnusamy, M.; Pang, M.; Annamaraju, P. K.; Zhang, Z.; Gong, R.; Chin, Y. E.; Zhuang, S. Transglutaminase-1 protects renal epithelial cells from hydrogen peroxide-induced apoptosis through activation of STAT3 and AKT signaling pathways. *Am. J. Physiol.: Renal Physiol.* **2009**, *297*, F1361−F1370.

(30) Perelman, A.; Wachtel, C.; Cohen, M.; Haupt, S.; Shapiro, H.; Tzur, A. JC-1: alternative excitation wavelengths facilitate mitochondrial membrane potential cytometry. *Cell Death Dis.* **2012**, *3*, e430.